Biosensors and Bioelectronics 130 (2019) 367–373

Contents lists available at ScienceDirect

Biosensors and Bioelectronics

journal homepage: www.elsevier.com/locate/bios

A paper-based chemiresistive biosensor employing single-walled carbon nanotubes for low-cost, point-of-care detection

Yu Shen[a], Thien-Toan Tran[b], Sidharth Modha[b], Hideaki Tsutsui[c], Ashok Mulchandani[a,d,*]

[a] Department of Chemical and Environmental Engineering, University of California, Riverside, CA 92521, USA
[b] Department of Bioengineering, University of California, Riverside, CA 92521, USA
[c] Department of Mechanical Engineering, University of California, Riverside, CA 92521, USA
[d] Materials Science and Engineering Program, University of California, Riverside, CA 92521, USA

ARTICLE INFO

Keywords:
Paper-based
Low-cost
Chemiresistive
Biosensors
Single-walled carbon nanotubes
Point-of-care

ABSTRACT

Paper-based biosensors are promising for low-cost diagnostics. However, its widespread use has been hampered due to a lack of sensitive detection methods that can be easily implemented on paper substrates. On the other hand, single-walled carbon nanotubes (SWNTs) -based chemiresistive biosensors are gaining popularity as label-free, highly sensitive biosensors. However, traditional SWNT-based chemiresistors need to be more affordable for use in resource-limited settings. In this study, we report fabrication, optimization and analytical characterization of a chemiresistive biosensor on paper for label-free immunosensing. We synthesized a water-based ink using pyrene carboxylic acid (PCA) through non-covalent π-π stacking interaction between PCA and SWNTs. The PCA/SWNTs ink concentration can reach ~4 mg mL^{-1} and was stable at room temperature for one month. We introduced a combination of wax printing and vacuum filtration to fabricate the hydrophilic channels and the well-defined PCA/SWNTs ink deposition on paper in a facile manner requiring no additional masks or stencils. Specific antibodies were then functionalized on the PCA/SWNTs. Quantitative and selective detection of human serum albumin (HSA) is demonstrated with a limit of detection (LOD) of 1 pM. This low LOD is attributed to the porous structure of the paper surface, which can accommodate more SWNTs. Furthermore, the hydroxyl group-containing cellulose fibers help connect the SWNTs into an electrical network. The paper-based chemiresistive biosensor proposed here is easy to fabricate, and designed for rapid, sensitive and selective detection of HSA. This work provides a potential platform for automated, disposable paper-based biosensors with multiplexed detection capability and microfluidic controls.

1. Introduction

More than 95% of deaths in developing countries are due to the lack of cost-effective medical interventions (Lee et al., 2010). Accurate and affordable diagnostics are important in the medical care systems, especially in developing areas (Yager et al., 2006). Paper-based microfluidics is an emerging field of low-cost miniaturized analytical assays. Although there are some commercial paper-based analytical tools such as home pregnancy tests (Hu et al., 2014) and pH test strips (Foster and Gruntfest, 1937), it is only recently that paper has received increasing attention as a promising substrate for analytical uses in the laboratory (Martinez et al., 2007; Cheng et al., 2010; Hsu et al., 2014). Paper-based sensors have notable advantages: (1) easy fabrication; (2) minimum instrument requirements; (3) possible low-power mode due to its intrinsic wicking capability; (4) portability; (5) biocompatibility and biodegradability; and (6) low cost. Paper is also favorable in reducing the liquids convection effect (Nie et al., 2010b). In addition, the surface roughness and porosity of paper substrate lead to an increased surface area for depositing electrical material, resulting in improved sensor performance (Sarfraz et al., 2012). These features make paper a suitable substrate for disposable sensors with potential microfluidic controls.

Numerous detection principles are employed in paper-based biosensors such as optical/colorimetric, electro-chemiluminescent and electrochemical (Nery and Kubota, 2013). However, the majority of paper-based sensors are limited by a poor limit of detection (LOD) (Martinez et al., 2007), low sensitivity (Hossain and Brennan, 2011), and variation in analytical imaging tools from lab to lab (Ge et al., 2012). In addition, sensors with labeling require complicated handling and operation (Cheng et al., 2010). Electrochemical biosensors are advantageous for being insensitive to light and dust while providing high sensitivity and selectivity (Nie et al., 2010a).

* Corresponding author at: Department of Chemical and Environmental Engineering, University of California, Riverside, CA 92521, USA.
E-mail address: adani@engr.ucr.edu (A. Mulchandani).

https://doi.org/10.1016/j.bios.2018.09.041
Received 1 July 2018; Received in revised form 7 September 2018; Accepted 12 September 2018
Available online 13 September 2018
0956-5663/

Single-walled carbon nanotubes (SWNTs) are almost entirely composed of surface atoms, which enable them to be highly sensitive to chemical changes on the surface of the nanomaterial. The ultrahigh surface-to-volume ratio renders SWNTs a Debye length that is comparable to the size of the nanostructures, which causes significant modulation of their electronic properties upon exposure to analytes (Tang et al., 2017). Furthermore, the high charge mobility of SWNTs enables low-power operations. These properties enable label-free detection of analytes with higher sensitivities and lower LODs (Park et al., 2010; Rajesh et al., 2013; Tan et al., 2015). Therefore, the integration of paper-based chemiresistive biosensor employing SWNTs benefits from using both paper and SWNTs materials.

Technologies to fabricate paper-based channels include photolithography (Martinez et al., 2009), screen-printing (Dungchai et al., 2011), lacquer spraying with iron masks (Nurak et al., 2013), vacuum filtration with metal stencils (Lei et al., 2015), inkjet printing (Abe et al., 2008) and wax printing (Lu et al., 2009). Photolithography is the most precise technology to define hydrophilic channels at a high resolution of 186 ± 13 μm (Martinez et al., 2009). However, it requires expensive equipment and organic solvents. Abe et al. (2008) developed an inkjet printing method to deposit customized materials onto paper substrates. However, hydrophilic channels formation involved the use of highly hydrophobic polymers dissolved in organic solvent and a toluene etching agent. Screen-printing is a relatively simple method, but the resolution is limited to hundreds of micrometers and the inability to reuse the screens is environmentally unfriendly (Dungchai et al., 2009). Other cost-effective methods such as polydimethylsiloxane (PDMS) plotting (Bruzewicz et al., 2008) involve no organic solvents and photoresist but require customized plotters. The paraffin pen has also been employed to define paper-based hydrophobic barriers with low resolution in the centimeter range (Lee et al., 2016). Vacuum filtration is also employed where carbon ink is pre-functionalized with specific biorecognition element and deposited onto paper with small pore sizes using laser-cut metal masks followed by the formation of PDMS hydrophobic barriers (Lei et al., 2015). However, this method needs special and brittle paper materials with pore sizes of 200 nm (Lee et al., 2016) and 800 nm (Lei et al., 2015), limiting its robustness and wide application beyond the laboratory. Wax printing, on the other hand, has several merits (Lu et al., 2009) such as (1) simple fabrication process of printing and baking with adequate resolutions; (2) rapid fabrication (5–10 min); (3) low cost (paper and wax printer are easy to obtain) and (4) environmentally-friendliness (no organic solvent in the wax printing and disposability by incineration). These merits make the wax printing method widely compatible with various aqueous solutions of various pH values, acids, bases and glycerol (Carrilho et al., 2009). Hence, to overcome the aforementioned obstacles with other methods, a SWNT-based highly sensitive, label-free chemiresistive biosensors on paper using wax printing and vacuum filtration techniques were explored in this study. Selective and quantitative detection of a target analyte, human serum albumin (HSA), demonstrated the excellent sensing ability of the proposed paper-based chemiresistor biosensor platform. The fabrication method in this work provides prospective simplification in paper-based chemiresistive biosensor design and fabrication.

2. Materials and methods

2.1. Reagents and instruments

Pyrene carboxylic acid (PCA) was purchased from Tokyo Chemical Industry Co., Ltd. (Portland, OR, USA). SWNTs (grade P3) was purchased from Carbon Solutions, Inc. (Riverside, CA, USA). N, N-Dimethylformamide (DMF), acetone, (1-ethyl-3-(3-dimethylaminopropyl)carbodiimide hydrochloride) (EDC), N-hydroxysulfosuccinimide (NHS), and ethanolamine were purchased from Fisher Scientific (Chino, CA, USA). Methanol, Whatman 5 qualitative filter paper, human serum albumin (HSA), and bovine serum albumin (BSA) were purchased from Sigma-Aldrich Corp. (St. Louis, MO, USA). Tween 20 (100%) was purchased from Bio-Rad (Hercules, CA, USA). Monoclonal anti-HSA antibody was purchased from BiosPacific, Inc. (Emeryville, CA, USA). N_2 and NO_2 gas cylinders were obtained from Airgas (Riverside, CA, USA). Silver paste was purchased from Ted Pella, Inc. (Redding, CA, USA). Polytetrafluoroethylene (PTFE) membranes were obtained from Millipore Corp. (Burlington, MA, USA). Ultra-sonication was done using a Branson m1800 (Danbury, CT, USA). Wax printing was done using a Xerox ColorQube 8880 (Norwalk, CT, USA). Electrochemical work station CH Instrument 6005E (Austin, TX, USA) and Keithley 2636 system source meter (Tektronix, Beaverton, OR, USA) were used to collect electrical signals.

2.2. Synthesis and characterization of water-based PCA/SWNTs ink

A schematic flowchart of the water-based PCA/SWNTs ink is shown in Fig. S1a (see Supplementary information). In brief, 50 mg SWNTs powder and 25 mg PCA were dispersed in 25 mL DMF individually. Twenty minutes of ultra-sonication ensured good dispersion of SWNTs in DMF. SWNTs/DMF and PCA/DMF were well mixed with stirring for 12 h to achieve complete π-π stacking interaction. The mixture was then vacuum filtered by PTFE membranes to accumulate a wet cake of PCA/SWNTs. Consecutive washes with methanol and DI water removed excessive solvent and PCA. The PCA/SWNTs was collected and weighted carefully before re-dispersion in Milli-Q water to obtain a desired concentration.

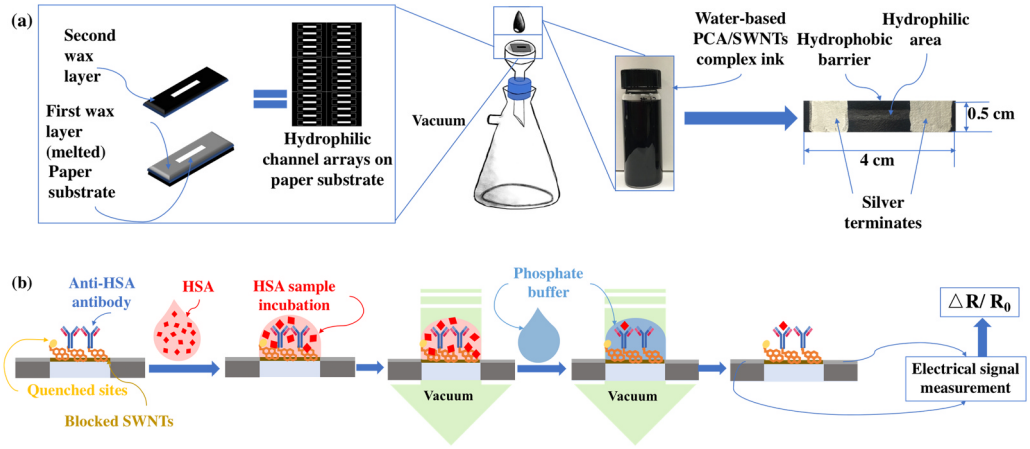

Fig. 1. Schematic of (a) wax printing and PCA/SWNTs ink deposition processes; (b) sensing protocol including sample incubation and PB wash process.

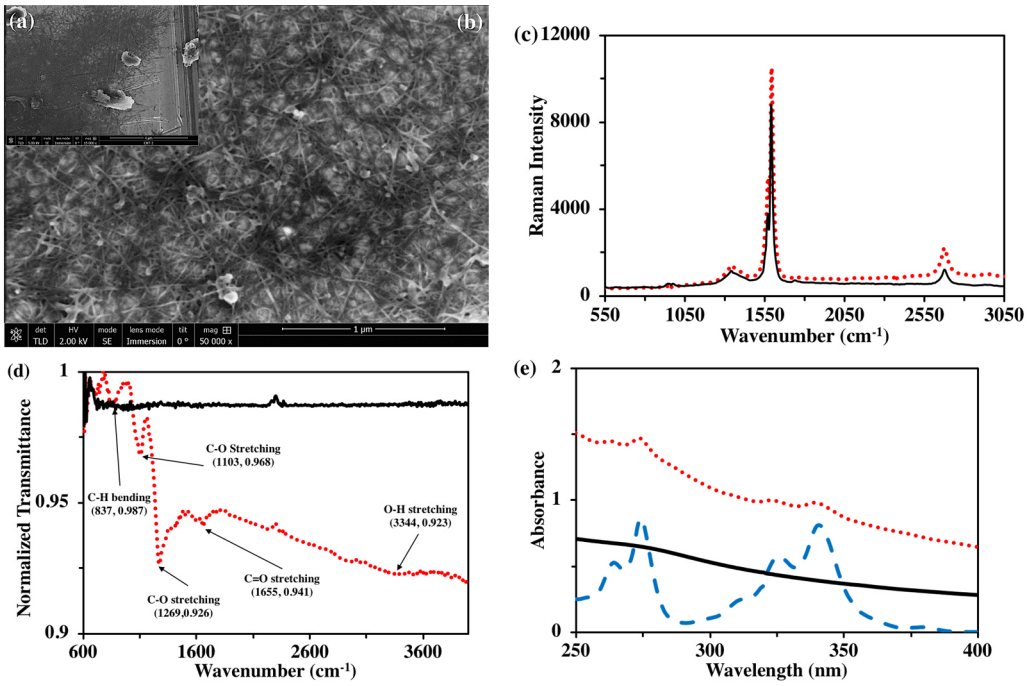

Fig. 2. Characterizations of water-based unmodified SWNTs and PCA/SWNTs ink. (a) SEM images of unmodified SWNTs/H_2O at < 0.1 mg mL^{-1}; (b) PCA/SWNTs in H_2O at ~4 mg mL^{-1}; (c), (d) and (e) are Raman spectrum, FTIR spectrum and UV–Vis spectrum of unmodified SWNTs (solid line), PCA/SWNTs (dotted line) and PCA/methanol (dashed line), respectively.

2.3. Wax printing and PCA/SWNTs ink deposition

The wax printing process is shown in Fig. 1**a**. Patterns were pre-designed on a computer using GIMP software. Fluidic channels (21 mm long and 1 mm wide) were created by printing the wax patterns onto the paper surface. Baking at 170 °C for 5 min melted the wax ink into the paper matrix, creating hydrophobic regions throughout the thickness of the paper. A second layer of the pattern was printed on the same side of the paper to ensure adequate hydrophobicity near the paper surface. The paper substrates were then placed at the center of a vacuum filter funnel under a vacuum pressure of ~78 kPa. A 3 mL syringe was used to transfer the PCA/SWNTs ink onto the paper surface. The vacuum forced the ink onto the paper while the wax barrier confined the ink to the sensing region. Silver paste was prepared in acetone at 2.15 g mL^{-1} and silver terminals were painted on each end of the sensing channel with a brush of 0.25 cm diameter. The terminals were subsequently dried at room temperature.

2.4. Preliminary NO_2 gas sensing

Fig. S1b (see Supplementary information) shows the set-up used for gas sensing. A gas chamber made of poly (methyl methacrylate) (PMMA) and PDMS gasket ensured the sealing of the chamber. NO_2 gas and N_2 gas were supplied from gas cylinders. Under the control of mass flow controllers (MFCs), NO_2 was diluted in a gas mixer with N_2 before approaching the PCA/SWNTs channels. Each pulse of NO_2 was 2 min and the N_2 recovery was 10 min. A LabView-controlled Keithley 2636B instrument applied 0.1 V across the source-drain electrodes and measured the source-drain current with respect to time.

2.5. Functionalization of anti-HSA antibody

All incubations were conducted in humid air with a wet Kimwipe around the sensors at room-temperature. Fifteen seconds of vacuum pressure at 78 kPa was adequate to remove 20 µL bulk fluid vertically through the sensing channels. Monoclonal anti-HSA antibodies were covalently attached to the carboxylic groups on the PCA/SWNTs by EDC/NHS chemistry. First, the sensing channels were immersed in 10 mM phosphate buffer (PB) (pH 6.2) containing 4 mM EDC and 8 mM NHS for 20 min to activate the carboxylic groups, followed by adequate 10 mM PB wash. Diluted anti-HSA antibody in 10 mM PB (pH 6.2) at 20 µg mL^{-1} was pipetted onto the sensing channels and incubated for 2 h followed by washing with 10 mM PB. Quenching and blocking agent were prepared in 10 mM PB (pH 6.2) and quenching of unreacted -NHS and blocking of bare SWNTs were completed by pipetting 0.1 M ethanolamine, with 10 mM PB washes, and 0.1% Tween 20, with 10 mM PB washes, respectively. Then the functionalized paper-based devices were ready for biosensing. The negative controls were fabricated with anti-HSA antibody on the sensor while sensing with 10 mM PB as blank samples for 6 times per sensor or 30 µM BSA. The positive control sensors were fabricated without antibody functionalization but with the quenching and blocking process with ethanolamine and Tween 20, respectively.

2.6. Sample incubation and electrochemical measurements

All electrochemical measurements were carried out with a CH Instrument (Model 6005E) and a Keithley source meter (Model 2636) at room temperature. Flat aluminum clips were used for connecting to the silver terminals. For NO_2 gas sensing, Keithley instrument obtained the long-time resistance records with a constant source-drain voltage at 0.1 V. For sensing liquid sample, the electrical measurements were done by measuring the I-V curve by sweeping the potential between source and drain using linear sweep voltammetry (LSV) from −0.1 V to 0.1V. The reciprocal of the slope of the I-V curve was the resistance of the sensing channels. All HSA standard solutions were prepared in 10 mM PB at a desired pH. BSA were prepared at 30 µM in 10 mM PB (pH 7.4) for the specificity study. Each time, 20 µL of analyte sample was pipetted onto the sensing channel. After 5 min incubation, vacuum force removed the bulk fluid and 10 mM PB (at the same pH value of the analyte samples) washes under vacuum removed unbound molecules (Fig. 1**b**).

3. Results and discussion

3.1. Characterization of PCA/SWNTs ink

PCA is one of the simplest molecules that contains both carboxylic

and pyrene groups and is thus an ideal bilinker molecule for facilitating both dispersion of SWNTs in aqueous media and its functionalization with biomolecules without affecting the electrical properties. SEM images in Fig. 2**a**, **b** show the distinct difference between unmodified SWNTs and the PCA modified SWNTs (from here on designated as PCA/SWNTs). The unmodified SWNTs at $< 0.1\ mg\ mL^{-1}$ formed large aggregates, whereas the PCA/SWNTs was more dispersed in water. This was attributed to the π-π stacking that occurs between the pyrene groups and the aromatic structures of SWNTs. The –COOH groups on the SWNTs provide the hydrophilic moiety with affinity to water. The PCA/SWNTs ink can be stable for up to one month at ambient condition (see Supplementary information, Fig. S6). The Raman spectrum in Fig. 2**c** shows the D-band and G-band of unmodified SWNTs and PCA/SWNTs at $1340\ cm^{-1}$ and $1595\ cm^{-1}$, respectively. The D-band is related to the disordered carbon bonding consistent with defects in the graphite lattice of the SWNTs (Brown et al., 2001). The ratio of D-band to G-band was 0.131 and 0.133 for the SWNTs before and after the PCA modification. The mild change in D-band to G-band ratio, compared to other SWNTs modification methods (Simmons et al., 2009), confirms that the PCA/SWNTs retained its mechanical and electrical properties during the non-covalent modification. The increased concentration of carboxylic groups on SWNTs was confirmed by the FTIR spectrum. The characteristic peaks are demonstrated in Fig. 2**d** where C-H bending and C-O, C = O, and O-H stretching are pointed out. Fig. 2**e** also reveals the UV–Vis spectrum of unmodified SWNTs in H_2O, PCA/SWNTs in H_2O and PCA in methanol. PCA in methanol showed two characteristic peaks at 274 nm and 341 nm. Clearly, the unmodified SWNTs showed no obvious peaks, whereas the PCA/SWNTs showed the absorption peaks corresponding to PCA moieties. These results validated the successful non-covalent modification of PCA on SWNTs, allowing a higher concentration of carboxylic moieties on SWNTs. This method enabled a higher dispersibility of carbon nanotubes in water and a higher density of bio-conjugation sites for antibody functionalization. Moreover, since the π-π interaction between SWNTs and the pyrene structure of PCA is universal among SWNTs and analogous aromatic ring-containing molecules, this fabrication method provides great potential in the development of non-covalent functionalization of SWNTs with a variety of bilinker molecules.

3.2. SWNTs transducing element fabrication and optimization

As is shown in Fig. 1**a**, simple vacuum filtration facilitated the maskless deposition of PCA/SWNTs ink on paper substrates. The second layer of wax on the paper surface prevented flooding of the PCA/SWNTs ink during the deposition process. By varying the volume of PCA/SWNTs ink, the initial resistance of the transducing element can be tuned. Fig. 3**a** demonstrates that increasing loading of the PCA/SWNTs decreased the initial resistance. Fig. S2 (see Supplementary information) displays the I-V curves of various loadings of PCA/SWNTs in the hydrophilic channels. When the concentration exceeded $10\ \mu g\ mm^{-2}$, the resistance plateaued. However, the thickness of the PCA/SWNTs layer displays a linear relationship with respect to the PCA/SWNTs loading.

The combination of wax printing and vacuum filtration in this study is beneficial compared to previous studies utilizing the vacuum filtration method. Lee et al. (2016) and Lei et al. (2015) developed a multi-step method to define the sensing regions on paper, in which metal masks are necessary to define the geometry of the carbon materials on paper, followed by time-consuming hydrophobic barrier formation. For example, PDMS formed hydrophobic barrier throughout the thickness of carbon material layers and paper substrate after hours of curing at low temperature (4 °C) to slow the polymerization of PDMS before it finally penetrated to the other side of the paper. Thus, the locations of carbon materials and hydrophilic sensing areas were formed separately. On the other hand, in our method, the determination of hydrophilic sensing areas and the PCA/SWNTs ink deposition on paper were created in a consistent way where no mask/stencil was needed. Therefore, this method eased the equipment requirements and eliminated the need of gaskets for sealing since wax printed barriers were adequate to ensure well-defined geometries of both the hydrophilic area and PCA/SWNTs geometry on paper.

It is reported that the initial resistance of the chemiresistor affects the biosensor sensitivity (Zhang et al., 2007). To achieve the highest sensitivity in the transducing element, we evaluated the performance of our paper-based chemiresistor for sensing of NO_2 gas. Fig. 3**b**, **c** shows the responses and optimization of initial resistance of transducer resistance. When exposed to NO_2, the p-doped semiconducting SWNTs shifted the Fermi level closer to the valence band. This lead to enriched hole carriers in the SWNTs and increased the conductance (Kong et al., 2000). The optimum initial resistance before bio-functionalization for the PCA/SWNTs transducing element was between 4.5 kΩ to 5.5 kΩ. Accordingly, all subsequent devices were fabricated with initial resistance within this range.

3.3. Biosensor fabrication, optimization and analytical characteristics

Fig. S3 (see Supplementary information) shows I-V curves of the device after each modification step during the biosensor fabrication process. The initial resistances were all within the range of $5.0 \pm 0.38\ k\Omega$ (n = 6), indicating good repeatability of the SWNTs chemiresistor transducer fabrication process using our new maskless method. After incubation with 10 mM PB (pH 6.3) the resistance increased by ~10% (Fig. 4). This is probably because more water molecules in the buffer adsorbed into the SWNT network and behaved similar to electron donors, which reduced the hole density of p-type SWNTs (Han et al., 2012). As shown in Fig. 4, while the resistance changes were not significant after the EDC/NHS chemistry and the quenching/blocking processes, there was a dramatic increase upon antibody functionalization. These results prove successful functionalization of antibodies on the sensing channels.

Next, we evaluated the performance of anti-HSA functionalized SWNTs chemiresistor on paper for detection of HSA. The result showed that the biosensor current decreased, i.e. the resistance increased, with increasing concentration of HSA (Fig. S4) over a broad dynamic range from 0 to ~50 nM HSA. In this study, the analyte sample was incubated for 5 min and the biosensor was washed in between incubation with increasing concentration of analyte sample with a 60 µL single bulk wash of 10 mM PB.

The response of the paper-based chemiresistor biosensor is a function of the volume of buffer wash to remove any free antigen. Two methods of biosensor washing with 10 mM PB post incubation with successive increasing concentration of HSA – a single bulk wash with 60 µL and three washings with 20 µL each - were investigated. A comparison of normalized resistance change $[(R - R_O)/R_O$, where R_O is the resistance of the device after functionalization, quenching and blocking and R is the resistance after incubation with sample] between a single/bulk wash and multiple washes with smaller volumes showed the bulk wash to be equally efficient as multiple washes (Fig. 5**a**). This is probably due to the buffer washes traversing vertically through the SWNTs thickness instead of being diffusion-dependent. This finding is also important as a single wash makes the analysis simple to conduct.

The duration of incubation/immunoreaction of the analyte sample with the biosensor can affect the sensor/chemiresistor sensitivity. A comparison of the biosensor responses for incubation times of 5 and 10 min showed (Fig. 5**b**) the difference in the sensitivity to be statistically insignificant ($p \approx 0.45 > 0.05$). Therefore, an incubation time of 5 min was selected for subsequent experiments.

The effect of varying amounts of anti-HSA employed for functionalization of SWNTs channel on the biosensor sensitivity and dynamic range was investigated. As shown in Fig. 5**c**, while the biosensor sensitivity, slope of the plot of normalized resistance change versus HSA concentration increased by 25% when the amount of anti-HSA used for

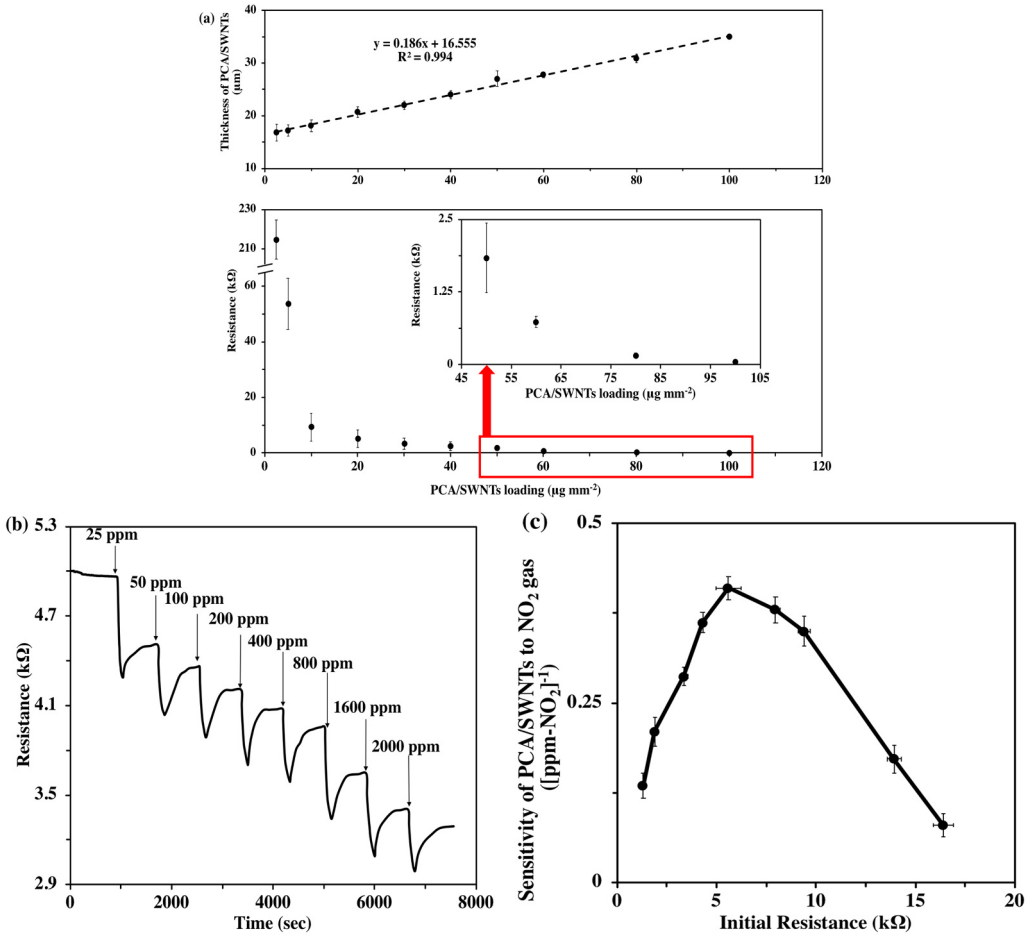

Fig. 3. Preliminary optimization of PCA/SWNTs density on the sensing channels. (a) The relationships between the loading of PCA/SWNTs on paper versus the initial resistance, and a linear relationship between the thickness and the loading of PCA/SWNTs. Each data point is an average of 6 devices and the error bars represent ± 1 standard deviation; (b) A typical response of PCA/SWNTs to NO_2 gas, with arrows indicate the exposure to NO_2 gas; (c) the changing sensitivity with various initial resistances. Each data point is an average of 9 sensors and the error bars represent ± 1 standard deviation.

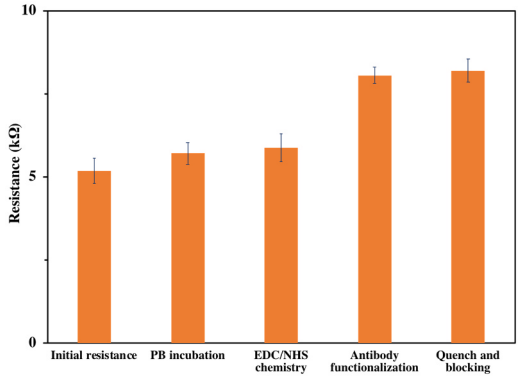

Fig. 4. Resistances change of the paper-based SWNTs chemiresistor device during the different functionalization steps of biosensor fabrication. The data points in the inset are average of 6 devices and error bars represent ± 1 standard deviation.

biofunctionalization was increased from 0.2 to 0.4 μg, there was only a 2% gain in sensitivity when the anti-HSA amount was increased further to 0.8 μg per device. A reason might be that the limited bio-conjugation sites on the PCA/SWNTs channels and the dosage of 0.4 μg anti-HSA antibody per device nearly saturated the available bio-functionalization sites, and therefore no significant further improvement in the sensitivity was seen. Based on these results, the amount of 0.4 μg anti-HSA per device was used in subsequent experiments.

The analytical figures of merits (sensitivity, selectivity and controls) for the present biosensor were obtained from calibration plots prepared using devices with optimized amount of anti-HSA (0.4 μg per device), incubation time of 5 min with 20 μL of analyte sample with 0 to ~50 nM of HSA and a 60 μL bulk wash with 10 mM PB (Fig. 5). As shown in the figure, the response was a linear function of the log of HSA over the range of 0.015–9.43 nM with a sensitivity of 9.44% change per Log_{10}([HSA, nM]). The LOD estimated by S/N = 3 was 1 pM HSA. The sensors had excellent reproducibility as evidenced by a low coefficient of variation, 6.67–8.97% of the data points obtained from 12 independent sensors with 0.4 μg antibody per device. In comparison with traditional sensors on the detection of HSA, most of these detection limits were in micromolar range (Choi et al., 2004). The increased sensitivity is probably due to the porous and rough surface of the paper substrate compared to smooth surface of Si wafer or glass substrate (Ogata et al., 2017). Thus, paper substrate can accommodate more SWNTs with a firm connectivity of SWNTs on paper (Tsai et al., 2016). The cellulose fibers contain multiple hydroxyl groups that form hydrogen bonds not only between cellulose molecules, but also with SWNTs. Thus, disconnected SWNTs on paper matrix are electrically bridged even though the paper fiber is dielectric. The carrier hopping and tunneling effects facilitate the inter-tube conduction, which leads to an increased percolation path and decreased effective conduction distance (Han et al., 2012). As a result, the paper-based biosensor sensitivity was increased.

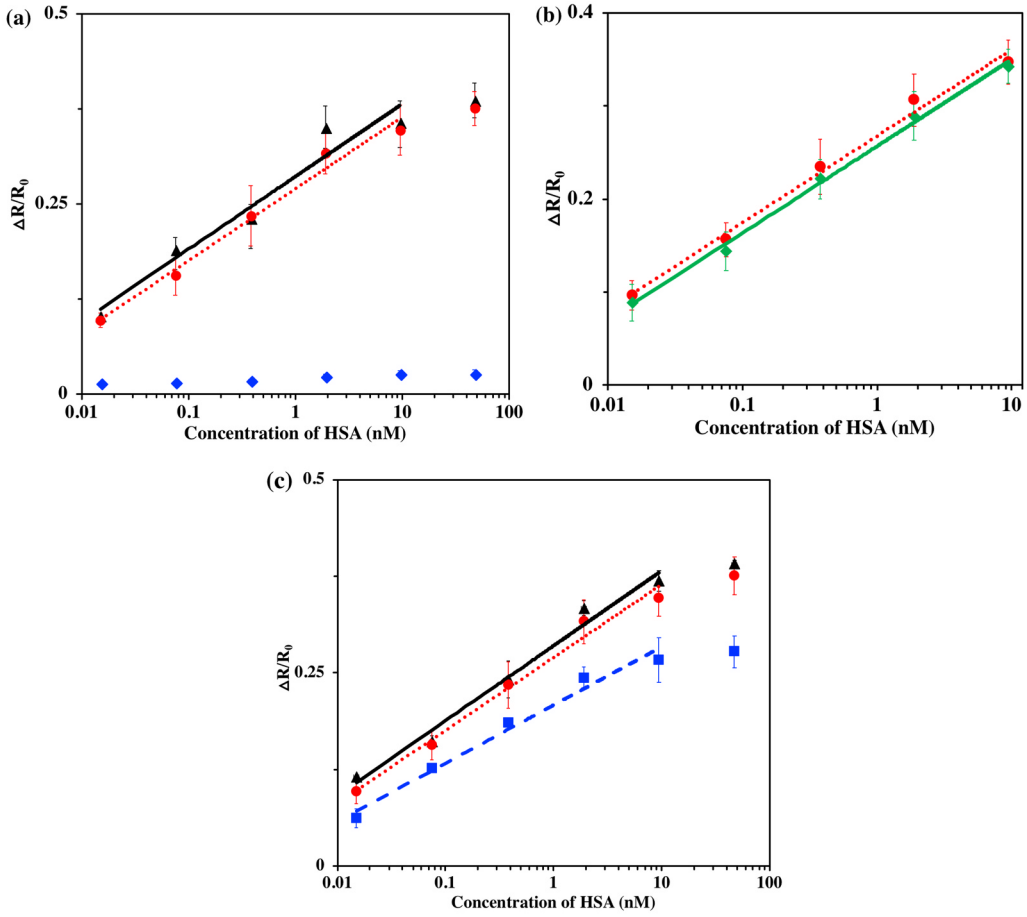

Fig. 5. The change of the electrical properties of the sensing channels at increasing concentrations. (a) Relative resistance changes for bulk wash mode (•) with linear regression y = 0.0944 Log_{10} (x) + 0.270 with R^2 = 0.984, individual wash mode (▲) with linear regression y = 0.0957 Log_{10} (x) + 0.286 with R^2 = 0.952, and control (◆). Each data point is an average of 12 sensors; (b) Comparison of 5 min (•) and 10 min (◆) HSA sample incubation in PB, with regression lines for 5 min HSA incubation (dotted line) y = 0.0944 Log_{10} (x) + 0.2672 with R^2 = 0.991, and for 10 min HSA incubation (solid line) y = 0.0932 Log_{10} (x) + 0.2566 with R^2 = 0.996. Each data point is an average of 6 sensors. All error bars represent ± 1 standard deviation. (c) Comparison of different amount of anti-HSA antibody used in the bio-functionalization process: 0.2 µg (■) with linear regression y = 0.0754 Log_{10} (x) + 0.209 with R^2 = 0.979 and 0.4 µg (•) with linear regression y = 0.0944 Log_{10} (x) + 0.270 with R^2 = 0.984 and 0.8 µg (▲) with linear regression y = 0.0971 Log_{10} (x) + 0.285 with R^2 = 0.981. Each data point is an average of 9 sensors. All error bars represent ± 1 standard deviation.

The positive control experiment, in which the sensor without anti-HSA antibody was exposed to 0 to ~ 50 nM HSA (Fig. 5a) showed the biosensor had a minimal response to their exposures confirming the high quality of sensors prepared by the transducer fabrication and biofunctionalization protocol developed in this work. Additional negative control experiment in which a biosensor with anti-HSA antibody was exposed to blank PB, i.e. no HSA, repeatedly for 6 times, had a response of +3.15 ± 0.56% (Fig. S5, see Supplementary information). The result of repeated vacuum filtrations validated that the observed response of biosensor to HSA was not caused by mechanical disruption in the SWNTs network. Furthermore, the negative control experiments in which the biosensor with anti-HSA antibody was challenged with 30 µM BSA in PB showed a response of +3.30 ± 0.40% (Fig. S5, see Supplementary information) confirmed the high selectivity of sensors for HSA.

3.4. Sensing mechanism of paper-based bulk SWNTs network biosensor

The sensing mechanisms of carbon nanotubes-based chemiresistive biosensors include electrostatic gating effect, changes in gate coupling, carrier mobility changes, and Schottky barrier effects (Heller et al., 2008). SWNTs-based field-effect transistor is usually dominated by a combination of electrostatic gating and Schottky barrier effect. In order to determine the dominating mechanism in our biosensors, we investigated the biosensor response to HSA samples in 10 mM PB at different pH values. As shown in Fig. 6, the response of the biosensors reversed (i.e. there was a decrease in resistance instead of an increase) when the sample pH dropped from 7.4 to 3.5. This is in accordance with observations of Heller et al. (2008), and is attributed to the change in the net charge of protein from negative to positive when the pH changed from above to below pI value, which for HSA is 4.8.

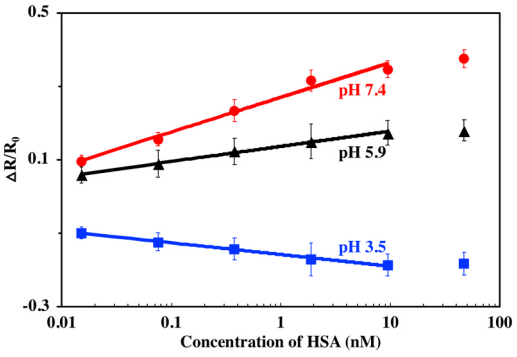

Fig. 6. The chemiresistive responses to HSA samples at different pH values: pH 7.4 (•), pH 5.9 (▲), and pH 3.5 (■). Each data point is an average of 9 sensors and the error bars represent ± 1 standard deviation.

Additionally, the magnitude of response was larger in pH 7.4 compared to 5.9 and is ascribed to the more negative charge of protein. Furthermore, it was observed that at pH 3.5 the magnitude of the response was smaller than that of pH 5.9 and is attributed to the dramatic decrease of the binding constant at pH below 4 (Sada et al., 1986). These results confirmed the dominating mechanism behind the paper-based SWNT-chemiresistive biosensors should be the electrostatic gating effect.

4. Conclusions

In conclusion, this study presents a low cost, yet highly sensitive SWNTs-based chemiresistive biosensor on paper. The biosensor is fabricated using a facile maskless method of combining wax printing and

vacuum filtering of water-based high concentration (4 mg/mL) and stable (up to one month under ambient conditions) SWNTs ink on the sensing channel followed by covalent biofunctionalization with bioreecognition molecule. With optimizations of the washing mode and the anti-HSA loading, detection of as low as 1 pM HSA with high selectivity was achieved with our paper-based biosensor.

This study verified the feasibility of the paper-based chemiresistor biosensor architecture with the proposed vertical-microfluidic channel. Furthermore, the synthesized water-based ink will be compatible with a spectrum of other instrumentation for chemiresistor biosensor fabrication since water is more instrument-friendly. The simple maskless method of wax printing and vacuum filtration will further ease the instrumental burden of traditional microfluidic channel fabrication on paper. Collectively, this work provides a potential platform for future automated, disposable paper-based biosensors with multiplexed detection capability and self-driven microfluidic controls towards meeting "ASSURED" (i.e. Affordable, Sensitive, Specific, User-friendly, Rapid and robust, Equipment-free, Deliver to the users who need them) criteria sought for diagnostics technologies in resource limited environment.

Acknowledgements

This work was supported by the National Science Foundation, USA, Grant 1606181. AM acknowledges the financial support of W. Ruel Johnson Chair.

Appendix A. Supporting information

Supplementary data associated with this article can be found in the online version at doi:10.1016/j.bios.2018.09.041.

References

Abe, K., Suzuki, K., Citterio, D., 2008. Anal. Chem. 80 (18), 6928–6934.
Brown, S., Jorio, A., Dresselhaus, M., Dresselhaus, G., 2001. Phys. Rev. B 64 (7), 073403.
Bruzewicz, D.A., Reches, M., Whitesides, G.M., 2008. Anal. Chem. 80 (9), 3387–3392.
Carrilho, E., Martinez, A.W., Whitesides, G.M., 2009. Anal. Chem. 81 (16), 7091–7095.
Cheng, C.M., Martinez, A.W., Gong, J., Mace, C.R., Phillips, S.T., Carrilho, E., Mirica, K.A., Whitesides, G.M., 2010. Angew. Chem. Int. Ed. 49 (28), 4771–4774.
Choi, S., Choi, E.Y., Kim, H.S., Oh, S.W., 2004. Clin. Chem. 50 (6), 1052–1055.
Dungchai, W., Chailapakul, O., Henry, C.S., 2009. Anal. Chem. 81 (14), 5821–5826.
Dungchai, W., Chailapakul, O., Henry, C.S., 2011. Analyst 136 (1), 77–82.
Foster, L.S., Gruntfest, I.J., 1937. J. Chem. Educ. 14 (6), 274.
Ge, L., Wang, S., Song, X., Ge, S., Yu, J., 2012. Lab Chip 12 (17), 3150–3158.
Han, J.-W., Kim, B., Li, J., Meyyappan, M., 2012. J. Phys. Chem. C 116 (41), 22094–22097.
Heller, I., Janssens, A.M., Männik, J., Minot, E.D., Lemay, S.G., Dekker, C., 2008. Nano Lett. 8 (2), 591–595.
Hossain, S.Z., Brennan, J.D., 2011. Anal. Chem. 83 (22), 8772–8778.
Hsu, C.-K., Huang, H.-Y., Chen, W.-R., Nishie, W., Ujiie, H., Natsuga, K., Fan, S.-T., Wang, H.-K., Lee, J.Y.-Y., Tsai, W.-L., 2014. Anal. Chem. 86 (9), 4605–4610.
Hu, J., Wang, S., Wang, L., Li, F., Pingguan-Murphy, B., Lu, T.J., Xu, F., 2014. Biosens. Bioelectron. 54, 585–597.
Kong, J., Franklin, N.R., Zhou, C., Chapline, M.G., Peng, S., Cho, K., Dai, H., 2000. Science 287 (5453), 622–625.
Lee, C.-Y., Lei, K.F., Tsai, S.-W., Tsang, N.-M., 2016. BioChip J. 10 (3), 182–188.
Lee, W.G., Kim, Y.-G., Chung, B.G., Demirci, U., Khademhosseini, A., 2010. Adv. Drug Deliv. Rev. 62 (4–5), 449–457.
Lei, K.F., Yang, S.-I., Tsai, S.-W., Hsu, H.-T., 2015. Talanta 134, 264–270.
Lu, Y., Shi, W., Qin, J., Lin, B., 2009. Anal. Chem. 82 (1), 329–335.
Martinez, A.W., Phillips, S.T., Butte, M.J., Whitesides, G.M., 2007. Angew. Chem. Int. Ed. 46 (8), 1318–1320.
Martinez, A.W., Phillips, S.T., Whitesides, G.M., Carrilho, E., 2009. Anal. Chem. 82 (1), 3–10.
Nery, E.W., Kubota, L.T., 2013. Anal. Bioanal. Chem. 405 (24), 7573–7595.
Nie, Z., Deiss, F., Liu, X., Akbulut, O., Whitesides, G.M., 2010a. Lab Chip 10 (22), 3163–3169.
Nie, Z., Nijhuis, C.A., Gong, J., Chen, X., Kumachev, A., Martinez, A.W., Narovlyansky, M., Whitesides, G.M., 2010b. Lab Chip 10 (4), 477–483.
Nurak, T., Praphairaksit, N., Chailapakul, O., 2013. Talanta 114, 291–296.
Ogata, A.F., Edgar, J.M., Majumdar, S., Briggs, J.S., Patterson, S.V., Tan, M.X., Kudlacek, S.T., Schneider, C.A., Weiss, G.A., Penner, R.M., 2017. Anal. Chem. 89 (2), 1373–1381.
Park, M., Cella, L.N., Chen, W., Myung, N.V., Mulchandani, A., 2010. Biosens. Bioelectron. 26 (4), 1297–1301.
Rajesh, Sharma, V., Puri, N.K., Singh, R.K., Biradar, A.M., Mulchanadani, A., 2013. Appl. Phys. Lett. 103 (20), 203703.
Sada, E., Katoh, S., Sukai, K., Tohma, M., Kondo, A., 1986. Biotechnol. Bioeng. 28 (10), 1497–1502.
Sarfraz, J., Tobjork, D., Osterbacka, R., Linden, M., 2012. IEEE Sens. J. 12 (6), 1973–1978.
Simmons, T.J., Bult, J., Hashim, D.P., Linhardt, R.J., Ajayan, P.M., 2009. ACS Nano 3 (4), 865–870.
Tan, F., Saucedo, N.M., Ramnani, P., Mulchandani, A., 2015. Environ. Sci. Technol. 49 (15), 9256–9263.
Tang, R., Shi, Y., Hou, Z., Wei, L., 2017. Sensors 17 (4), 882.
Tsai, J.-Z., Chen, C.-J., Settu, K., Lin, Y.-F., Chen, C.-L., Liu, J.-T., 2016. Biosens. Bioelectron. 77, 1175–1182.
Yager, P., Edwards, T., Fu, E., Helton, K., Nelson, K., Tam, M.R., Weigl, B.H., 2006. Nature 442 (7101), 412.
Zhang, T., Mubeen, S., Bekyarova, E., Yoo, B.Y., Haddon, R.C., Myung, N.V., Deshusses, M.A., 2007. Nanotechnology 18 (16), 165504.